Temperature and atmospheric CO_2 concentration estimates through the PETM using triple oxygen isotope analysis of mammalian bioapatite

Alexander Gehler[a,1], Philip D. Gingerich[b,c], and Andreas Pack[d]

[a]Geowissenschaftliches Zentrum, Geowissenschaftliches Museum, Georg-August-Universität, D-37077 Göttingen, Germany; [b]Department of Earth and Environmental Sciences, University of Michigan, Ann Arbor, MI 48109; [c]Museum of Paleontology, University of Michigan, Ann Arbor, MI 48109; and [d]Geowissenschaftliches Zentrum, Abteilung Isotopengeologie, Georg-August-Universität, D-37077 Göttingen, Germany

Edited by Mark H. Thiemens, University of California, San Diego, La Jolla, CA, and approved May 17, 2016 (received for review September 17, 2015)

The Paleocene–Eocene Thermal Maximum (PETM) is a remarkable climatic and environmental event that occurred 56 Ma ago and has importance for understanding possible future climate change. The Paleocene–Eocene transition is marked by a rapid temperature rise contemporaneous with a large negative carbon isotope excursion (CIE). Both the temperature and the isotopic excursion are well-documented by terrestrial and marine proxies. The CIE was the result of a massive release of carbon into the atmosphere. However, the carbon source and quantities of CO_2 and CH_4 greenhouse gases that contributed to global warming are poorly constrained and highly debated. Here we combine an established oxygen isotope paleothermometer with a newly developed triple oxygen isotope paleo-CO_2 barometer. We attempt to quantify the source of greenhouse gases released during the Paleocene–Eocene transition by analyzing bioapatite of terrestrial mammals. Our results are consistent with previous estimates of PETM temperature change and suggest that not only CO_2 but also massive release of seabed methane was the driver for CIE and PETM.

PETM | temperature | CO_2 concentration | mammals

The Paleocene–Eocene transition at about 56 Ma (1–3) is marked by an abrupt climate change in conjunction with a large negative carbon isotope excursion (CIE), ocean acidification, and enhanced terrestrial runoff—during a period lasting less than 220,000 y (e.g., refs. 4–7). During the CIE a global temperature increase of 5–8 °C has been inferred from a variety of marine and terrestrial proxies (e.g., refs. 3 and 8–21), hence the name "Paleocene–Eocene Thermal Maximum," or PETM is frequently applied to the transition interval.

The CIE is well-documented by proxy data, and it is largely accepted that it was caused by the addition of a large amount of ^{13}C-depleted carbon into the exogenic carbon cycle (ref. 22 and references therein). Considering the atmospheric CIE to be between –4 and –5‰ (ref. 22 and references therein and refs. 23 and 24), the suggested amount of carbon needed to cause this negative carbon isotope shift ranges between 2,200 and 153,000 Gt, a range depending on the isotope composition of the hypothesized carbon source and secondarily on the model approach used (22, 24–27). Possible carbon sources are biogenic methane (i.e., methane clathrates, $\delta^{13}C$ ~–60‰), thermogenic methane or permafrost soil carbon ($\delta^{13}C$ ~–30‰), carbon released due to wildfires or through desiccation and oxidation of organic matter due to drying of epicontinental seas ($\delta^{13}C$ ~–22‰), and mantle CO_2 ($\delta^{13}C$ ~–5‰) (22, 28).

A massive release of methane clathrates by thermal dissociation (29) has been the most convincing hypothesis to explain the CIE since it was first identified. However, a methane clathrate source is still debated, and an involvement of other carbon sources—exclusively or additionally—is widely discussed (e.g., refs. 22, 26, and 28).

Global warming during the CIE is attributed to radiative forcing due to increased concentrations of greenhouse gases, most likely CO_2 and/or CH_4, and to accessory phenomena such as aerosol forcing and reduced cloudiness (26, 30).

Substantially different CO_2 scenarios have been discussed for the PETM. Mass balance estimates range from an increase in atmospheric CO_2 concentration of less than 100 ppm to an increase of several 10,000 ppm, depending on the proposed magnitude of the CIE and the associated carbon source (10, 22, 24, 25, 27, 31–34).

Existing proxy data for CO_2 concentrations in the time interval surrounding the PETM (50–60 Ma) suggest background partial pressure of CO_2 (pCO_2) levels between 100 and 1,900 ppm (ref. 35 and references therein). Only a single estimate (36) of the previously published data is questionably correlated to PETM strata (670 ppm).

From increased insect herbivory during the PETM Currano et al. (37, 38) suggested a three- to fourfold increase in atmospheric CO_2 but left open the possibility that increased herbivory was an effect of higher insect diversity and density due to the elevated temperature.

Here we bring evidence to bear on both temperatures and CO_2 concentrations through the Paleocene–Eocene transition based on triple oxygen isotope measurements ($\delta^{17}O$, $\delta^{18}O$) of bioapatite in mammalian tooth enamel.

The oxygen isotopic composition of mammalian body water is determined by its oxygen sources and sinks (Figs. S1 and S2). The main oxygen input sources for mammals are drinking water, food water, and inhaled air O_2. Sinks are feces, sweat, water loss due to transpiration, as well as exhaled CO_2 and moisture. The fractionation between $\delta^{18}O$ of body water and $\delta^{18}O$ of bioapatite in mammals is constant due to a constant body temperature of ~37 °C, and it has been demonstrated that it is possible to relate the $\delta^{18}O$ of mammalian bioapatite to the oxygen isotope composition of drinking water (i.e., environmental surface water, $\delta^{18}O_{SW}$) by empirically developed calibration equations or by modeling approaches (39–44). Due to the strong correlation between $\delta^{18}O_{SW}$ and mean annual (air) temperatures (MAT) (45), it is in turn possible to infer paleotemperatures using the oxygen isotope composition of $\delta^{18}O_{SW}$ reconstructed from $\delta^{18}O$ of mammalian bioapatite. This was first applied extensively by Bryant et al. (46).

Significance

Our data suggest that the sudden rise in atmospheric temperature during the Paleocene–Eocene transition was not accompanied by highly elevated carbon dioxide concentrations >~2,500 ppm. Instead, the low $^{13}C/^{12}C$ isotope ratios during the Paleocene–Eocene Thermal Maximum were most likely caused by a significant contribution of methane to the atmosphere. We present data applying a newly developed partial pressure of CO_2 proxy.

Author contributions: A.G., P.D.G., and A.P. designed research; A.G. performed research; P.D.G. contributed sample material; A.G., P.D.G., and A.P. analyzed data; and A.G., P.D.G., and A.P. wrote the paper.

The authors declare no conflict of interest.

This article is a PNAS Direct Submission.

[1]To whom correspondence should be addressed. Email: agehler@gwdg.de.

This article contains supporting information online at www.pnas.org/lookup/suppl/doi:10.1073/pnas.1518116113/-/DCSupplemental.

Table 1. Oxygen isotope composition ($\delta^{18}O_{PO4}$, $\Delta^{17}O_{PO4}$) of tooth enamel from second molars of *Ectocion osbornianus* and *Ectocion parvus* from the Clarks Fork Basin in north-western Wyoming

Species	Biozone	Level, m	Locality	Sample no.	$\delta^{18}O_{PO4}$, ‰	$\Delta^{17}O_{PO4}$, ‰	*N*	pCO_2 (model), ppm by volume		pCO_2 (model, 2.3× GPP), ppm by volume	
E. osbornianus	Wa-2	1,720	SC-2	85906	13.0 ± 0.4	−0.17 ± 0.04	5	500	−400 +600	1,150	−1,000 +1,400
E.osbornianus	Wa-2	1,720	SC-2	66572 (sample A)	12.4 ± 0.3	−0.18 ± 0.02	8	625	−400 +600	1,440	−1,000 +1,400
E.osbornianus	Wa-2	1,720	SC-2	66572 (sample B)	13.0 ± 0.5	−0.19 ± 0.03	7	750	−400 +600	1,730	−1,000 +1,400
Mean					12.8 ± 0.2	-0.18 ± 0.02	20	630	−230 +350	1,450	−500 +800
E.osbornianus	Wa-2	1,665	SC-161	80705	13.5 ± 0.4	−0.14 ± 0.02	3	225	−200 +400	520	−500 +1,000
E.osbornianus	Wa-2	1,665	SC-161	98404	13.2 ± 0.3	−0.13 ± 0.03	4	200	−200 +400	460	−500 +1,000
E.osbornianus	Wa-2	1,665	SC-161	68200	12.3 ± 0.3	−0.15 ± 0.03	4	250	−250 +500	580	−600 +1,200
Mean					13.0 ± 0.2	-0.14 ± 0.02	11	230	−200 +320	530	−460 +750
E.parvus	Wa-0	1,520	SC-67	83478	14.3 ± 0.3	−0.15 ± 0.04	2	250	−200 +400	580	−500 +1,000
E.parvus	Wa-0	1,520	SC-67	87354	14.3 ± 0.6	−0.18 ± 0.03	5	625	−400 +600	1,440	−1,000 +1,400
E.parvus	Wa-0	1,520	SC-67	86572 (sample A)	15.1 ± 0.2	−0.17 ± 0.03	7	625	−400 +600	1,440	−1,000 +1,400
E.parvus	Wa-0	1,520	SC-67	86572 (sample B)	14.4 ± 0.3	−0.15 ± 0.03	2	250	−200 +400	580	−500 +1,000
Mean					14.5 ± 0.2	-0.16 ± 0.02	16	440	−160 +250	1,010	−400 +600
E.osbornianus	Cf-3	1,502	SC-107	66621	11.0 ± 0.5	−0.14 ± 0.03	11	250	−250 +500	580	−600 +1,200
E.osbornianus	Cf-3	1,495	SC-138	67243 (sample A)	13.7 ± 0.3	−0.16 ± 0.03	7	500	−400 +500	1,150	−1,000 +1,200
E.osbornianus	Cf-3	1,495	SC-138	67243 (sample B)	13.8 ± 0.6	−0.19 ± 0.05	4	825	−400 +600	1,900	−1,000 +1,400
E.osbornianus	Cf-3	1,485	SC-11	64726	12.1 ± 0.3	−0.14 ± 0.02	3	225	−200 +500	520	−500 +1,200
Mean					12.7 ± 0.2	−0.16 ± 0.02	25	450	−200 +260	1,040	−450 +600

The reported pCO_2 data were calculated for modern gross primary productivity (GPP) and 2.3× elevated GPP on basis of the mass balance model (for details, see *Supporting Information*). Uncertainty estimates are ±1σ SD.

These studies rely solely on $\delta^{18}O$ because, in nearly all terrestrial fractionation processes, $\delta^{18}O$ is correlated to $\delta^{17}O$ by the equation $\delta^{17}O \approx 0.52 \times \delta^{18}O$ (e.g., ref. 47 and references therein).

However, air O_2, which is one of the main oxygen sources of mammalian body water, carries an isotope anomaly in ^{17}O (48) that is related to mass independent processes in the stratosphere. The isotope anomaly of inhaled air O_2 is transferred to the body water and hence to mammalian bioapatite. The ^{17}O anomaly of air O_2 scales with atmospheric CO_2 level and gross primary productivity (GPP) (49), and thus triple oxygen isotope analyses of bioapatite from fossil mammals can be used as a paleo-CO_2 proxy (see ref. 50 for more details).

The magnitude of the ^{17}O anomaly in mammalian bioapatite is connected to the fraction of inhaled anomalous air O_2 in relation to the other oxygen sources. Due to higher specific metabolic rates (i.e., higher specific O_2 respiration), smaller mammals carry a higher portion of anomalous oxygen in their bioapatite than larger mammals (50).

Studies relying on the relationship of paleotemperature to $\delta^{18}O$ in mammalian bioapatite already exist for the Paleocene–Eocene transition in the Clarks Fork and Bighorn Basin (Wyoming) based on various mammalian taxa, targeting either the carbonate oxygen component ($\delta^{18}O_{CO3}$) of mammalian tooth enamel, the phosphate oxygen component ($\delta^{18}O_{PO4}$), or both in a combined approach (8, 17, 20, 21, 51–53).

In the present study, we combine this well-established $\delta^{18}O$ paleothermometer (e.g., refs. 39 and 40) with the recently published discovery of a connection between the triple oxygen isotope composition of mammalian bioapatite and atmospheric CO_2 concentration (50).

Materials and Methods

Samples. The most suitable taxa for an application of the approach described above should have a body weight as small as possible (to ensure a high proportion of inhaled anomalous air oxygen in respect to the other oxygen sources) but large enough (with respect to fossil samples) to provide an adequate amount of diagenetically unaltered sample material (i.e., tooth enamel) (e.g., refs. 54 and 55).

We sampled tooth enamel from teeth from jaws and isolated teeth of 11 individual specimens of the phenacodontid genus *Ectocion* (*Ectocion osbornianus* and *Ectocion parvus*) from the Clarks Fork Basin (Sand Coulee area) in northwestern Wyoming (e.g., refs. 56 and 57). The enamel was carefully hand-picked under a binocular microscope before pretreatment. The samples cover a time interval of several mammalian biozones, from the late Clarkforkian (Cf-3) to the early Wasatchian (Wa-2), encompassing the PETM. All samples were acquired from the collections of the Museum of Paleontology at the University of Michigan, Ann Arbor (localities SC-2, SC-11, SC-67, SC-107, SC-138, and SC-161). All were molded and cast before destructive sampling. Only second molars (M_2) were used for the present study to obtain the highest possible comparability.

Sample Pretreatment. To ensure analysis was limited to the phosphate oxygen isotope composition ($\delta^{18}O_{PO4}$), other oxygen-bearing components of the sample material (e.g., organic matter, sorbed water, structural carbonate, and OH^- groups) were removed by treating the tooth enamel in an Ar-flushed horizontal tube furnace for 10–15 min at 1,000 °C. Subsequently, the samples were cooled to below 100 °C while remaining in an Ar atmosphere, followed by immediate storage in a desiccator until analysis (50). This procedure follows Lindars et al. (58), who demonstrated safe removal of all of the unwanted compounds at temperatures between 850 and 1,000 °C. Ar is used to avoid exchange with atmospheric water, which was reported to be a problem by Lindars et al. (58) when heating samples to 1,000 °C in ambient air.

Triple Oxygen Isotope Analysis. Variations in the oxygen isotope ratios ($^{17}O/^{16}O$, $^{18}O/^{16}O$) are reported relative to the international isotope reference standard Vienna Standard Mean Ocean Water 2 in the form of the $\delta^{17}O$ and $\delta^{18}O$ notation (59). In mass-dependent (equilibrium or kinetic) fractionation processes, variations in $\delta^{17}O$ broadly correlate with variations in $\delta^{18}O$. To better display small deviations from an otherwise good correlation, the $\Delta^{17}O$ value has been introduced. We follow the definition scheme for $\Delta^{17}O$ as presented in Pack and Herwartz (60) with $\Delta^{17}O = 1{,}000*\ln(\delta^{18}O/1{,}000 + 1) - 0.5305*1{,}000*\ln(\delta^{18}O/1{,}000 + 1)$. The $\Delta^{17}O$ has been normalized to a revised composition of NBS 28 quartz with $\delta^{17}O = 5.03‰$ and $\delta^{18}O = 9.60‰$ ($\Delta^{17}O = -0.05‰$).

A slope derived from analytical data of terrestrial rocks and minerals as done in previous studies (50, 55) has not been used because of its arbitrary selection depending on the specific samples analyzed to obtain it. However, the data can easily be converted for comparison with results from other studies and/or other laboratories.

Oxygen was released from the samples by infrared laser fluorination (61) and analyzed by gas chromatography isotope ratio monitoring gas mass spectrometry in continuous flow mode (e.g., refs. 50, 55, and 62). Typically, ∼0.3 mg of pretreated fossil tooth enamel was loaded into an 18-pit polished Ni sample holder along with ∼0.3 mg of pretreated tooth enamel from a modern African Elephant (*Loxodonta africana*) as an internal standard and ∼0.2 mg NBS 28 quartz. Following evacuation and heating of the sample chamber to 70 °C for at least 12 h, fluorination was implemented by heating the samples with a SYNRAD 50 W CO_2 laser in a ∼20–30 mbar atmosphere of F_2 gas, purified

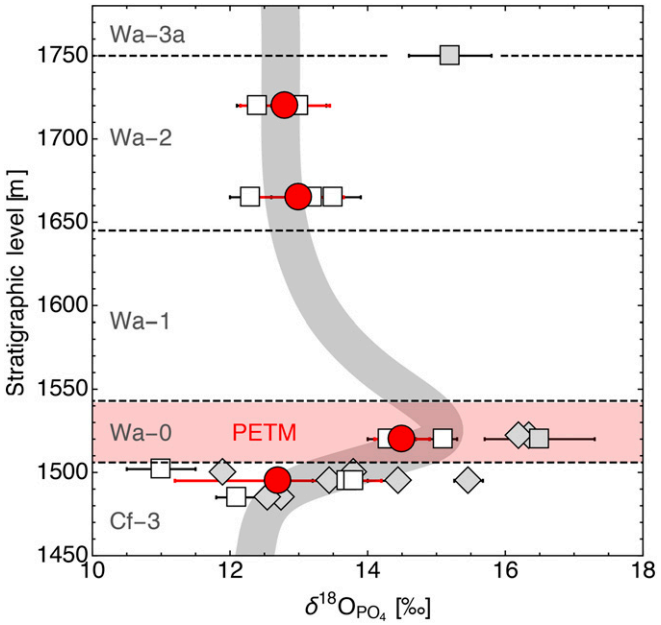

Fig. 1. Oxygen isotope composition ($\delta^{18}O_{PO4}$, ±1σ SD) of *Ectocion* (white squares, this study; Table 1), *Phenacodus* [gray diamonds; Secord et al. (20)], and *Coryphodon* specimens [gray squares; Fricke et al. (17)]. Red circles are mean values for *Ectocion* (this study). Missing error bars indicate single analyses. The stratigraphic level is expressed in meters above the K-T boundary in the Clarks Fork Basin. Age of *Ectocion* samples is in the range of –56 to –55 Ma (see Fig. 2).

according to Asprey (63). Liberated excess F_2 was reacted with heated NaCl (~180 °C) to NaF and Cl_2. The latter was cryotrapped by liquid N_2 until all samples were analyzed. Sample O_2 was cryofocused on a molecular sieve trap at –196 °C (liquid N_2) then expanded into a stainless steel capillary and transported with He as carrier gas through a second molecular sieve trap, where a fraction of the sample gas was again cryofocused at –196 °C. After releasing this back into the He carrier gas stream by heating it in a hot water bath (~92 °C), the sample O_2 was purified by passing it through a 5-Å molecular sieve GC column of a Thermo Scientific GasBench II and then injected via an open split valve of the GasBench II into the source of a Thermo MAT 253 gas mass spectrometer. The signals of $^{16}O^{16}O$, $^{17}O^{16}O$, and $^{18}O^{16}O$ were simultaneously monitored on three Faraday cups. Reference O_2 was injected before each sample measurement through a second open split valve of the GasBench II. Sample and reference gas peaks (m/z = 32) had an amplitude of 20–30 V.

The SD for replicates of the same bioapatite samples from different runs is typically better than ±0.5‰ in $\Delta^{18}O$ and ± 0.04‰ in $\Delta^{17}O$ for a single analysis.

A total of 72 single laser fluorination analyses were made using 14 different *Ectocion* tooth enamel samples (from the 11 *Ectocion* specimens used for the present study, 3 were sampled twice to have a reproducibility control between different analytical runs) (Table 1).

Results and Discussion

Temperature Change Across the PETM Inferred from $\delta^{18}O$ of *Ectocion* Tooth Enamel. The mean oxygen isotope composition of tooth enamel phosphate ($\delta^{18}O_{PO4}$) in the *Ectocion* specimens investigated increases by 2.2‰ from the late Clarkforkian (Cf-3) to the CIE in the early Wasatchian (Wa-0), considering the mean values for each mammalian biozone. From Wa-0 to Wa-2, a decrease in mean $\delta^{18}O_{PO4}$ of 1.6‰ is observed (different meter levels within Wa-2 do not show any difference in $\delta^{18}O_{PO4}$, so they were combined (Fig. 1 and Tables 1 and 2). This is in agreement with previous results from $\delta^{18}O_{PO4}$ (17, 20), as well as $\delta^{18}O_{CO3}$ (17, 20, 21) for mammals covering the same biozones in the same study area. To estimate the change of $\delta^{18}O_{SW}$ from $\delta^{18}O_{PO4}$, we used the relationship for modern herbivorous mammals ($\delta^{18}O_{SW} = 1.32 \times \delta^{18}O_{PO4}$), which Secord et al. (20) adapted from Kohn et al. (64).

Applying this to our results, $\delta^{18}O_{SW}$ became enriched by 2.9‰ from Cf-3 to Wa-0 followed by a depletion of 2.1‰ to Wa-2 (Table 2).

The $\delta^{18}O_{SW}$/MAT slope is sensitive to the latitudinal gradient and other factors (e.g., ref. 65), so an important precondition for estimating the corresponding change in temperature is to adjust this slope as closely as possible to early Cenozoic conditions. The modern temperature dependence for a MAT of 0–20 °C ranges between 0.5 and 0.6‰ per degree Celsius (66–68). During the Paleocene–Eocene transition in the Bighorn Basin, Secord et al. (20) proposed $\delta^{18}O_{SW}$/MAT slopes of 0.39 and 0.36 (per mille per degree Celsius), based on two different approaches.

For the *Ectocion* tooth enamel data of the present study, this implies an increase of 7.4 °C (8.1 °C) from Cf-3 to Wa-0 and a decrease of 5.4 °C (5.8 °C) from Wa-0 to Wa-2 (the value in parentheses refers to the slope for 0.36). These results are in general agreement with previous studies from Fricke et al. (17) and Secord et al. (20) based on tooth enamel $\delta^{18}O_{PO4}$ of *Coryphodon* and *Phenacodus*, respectively. Calculated on the same basis, the data from Fricke et al. (17) indicate a temperature increase of 6.2 °C (6.7 °C) from Cf-2 to Wa-0 and a decrease of 4.6 °C (5.0 °C) from Wa-0 to Wa-3. The data from Secord et al. (20) suggest a temperature increase of 7.2 °C (7.8 °C) from Cf-3 to Wa-0, if mean biozone values are used (Table 2).

Atmospheric CO_2 Levels Across the PETM Inferred from $\delta^{17}O$ of *Ectocion* Tooth Enamel. Tooth enamel of the investigated *Ectocion* specimens has a distinctly negative ^{17}O anomaly, with $\Delta^{17}O$ ranging between –0.19 and –0.13‰ (Table 1). The anomaly is due to the portion of oxygen in the bioapatite that comes from inhaled isotopically anomalous air O_2 (50). To estimate the $\Delta^{17}O$ of PETM air oxygen from the tooth enamel measurements, we used the oxygen mass balance model of Pack et al. (50), developed for terrestrial herbivorous mammals (for details see *Supporting Information*). The

Table 2. Estimated change in $\delta^{18}O_{SW}$ and temperature at the Paleocene–Eocene transition in the Clarks Fork and Bighorn Basin

Biozone interval	$\Delta^{18}O_{PO4}$, ‰	$\Delta^{18}O_{SW}$, ‰	ΔT (0.58‰/°C)	ΔT (0.39‰/°C)	ΔT (0.36‰/°C)
This study					
Wa-0 to Wa-2	−1.6	−2.1	−3.6	−5.4	−5.8
Cf-3 to Wa-0	+2.2	+2.9	+5.0	+7.4	+8.1
Secord et al. (20)					
Cf-3 to Wa-0	+2.1	+2.8	+4.8	+7.2	+7.8
Fricke et al. (17)					
Wa-0 to Wa-3a	−1.4	−1.8	−3.1	−4.6	−5.0
Cf-2 to Wa-0	+1.8	+2.4	+4.1	+6.2	+6.7

Based on $\delta^{18}O_{PO4}$ of *Ectocion* (this study), *Phenacodus* [Secord et al. (20)] and *Coryphodon* [Fricke et al. (17)], for three different MAT/$\delta^{18}O_{SW}$ slopes [the modern and two calculated values for early Eocene conditions from Secord et al. (20)].

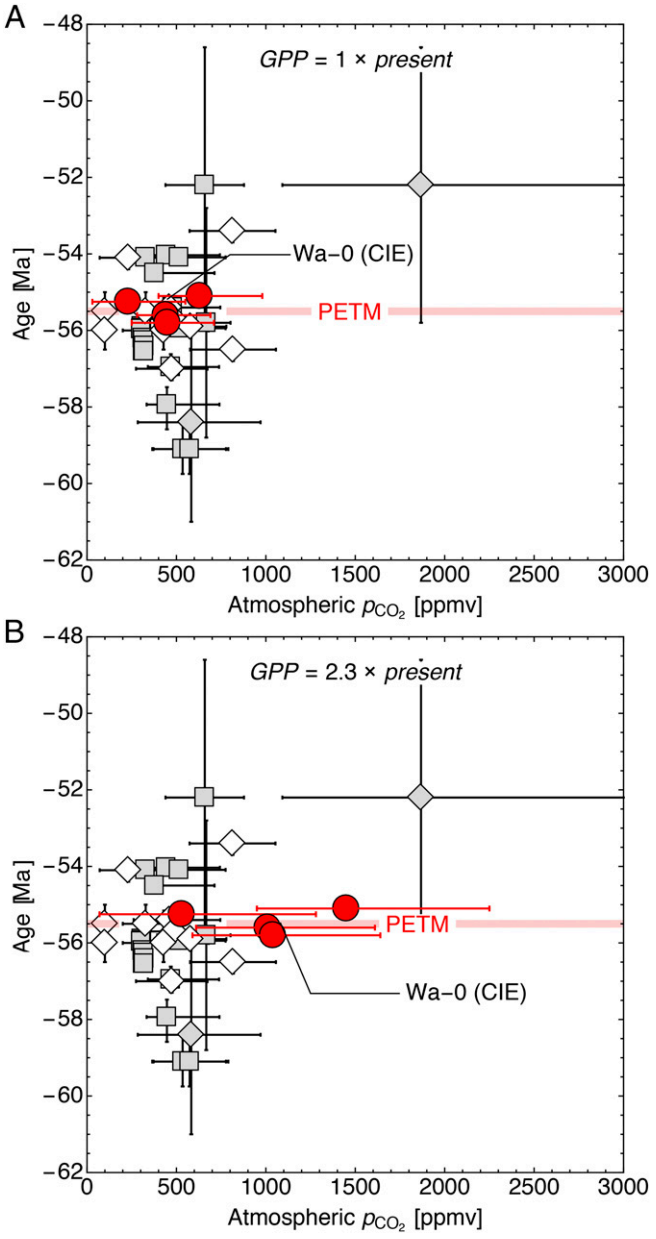

Fig. 2. Existing proxy data for pCO_2 between 50 and 60 Ma adapted from the compilation of Beerling and Royer (35), compared with pCO_2 estimates from $\Delta^{17}O$ of *Ectocion* bioapatite (red circles, this study). pCO_2 has been calculated for (*A*) modern global GPP conditions and (*B*) GPP 2.3 times the modern value, as proposed by Berner (71). White diamonds, paleosols; gray squares, leaf stomata; white squares, marine phytoplankton; gray diamonds, liverworts. pCO_2 results here are the first to our knowledge to come unquestionably from the PETM interval. Note that pCO_2 results for the PETM here are not elevated but consistent with earlier and later pCO_2 values reported by Beerling and Royer (35).

body weights of *E. osbornianus* and *E. parvus* are estimated to have been 9 and 5 kg, respectively (e.g., refs. 69 and 70).

Combining the approach of Pack et al. (50) with the linear relationship between $\Delta^{17}O_{air}$ and pCO_2 given by Bao et al. (49), the estimated mean pCO_2 values are 450, 440, 230, and 630 ppm for Cf-3 (1,485- to 1,502-m level), Wa-0 (1,520-m level), Wa-2 (1,665-m level), and Wa-2 (1,720-m level), respectively (Fig. 2*A* and Table 1). The uncertainty estimate is in the range of ± several hundred ppm. However, these numbers are based on modern O_2 and GPP conditions. Whereas pO_2 remains more or less unchanged within the last 60 Ma (71), a considerably different GPP of 2.3 times the modern value has been estimated by Beerling (72) for the early Eocene. Because a doubling of GPP results in a halving of $\Delta^{17}O_{air}$ (49, 50), a 2.3 GPP would imply pCO_2 mean values of 1,040, 1,010, 530, and 1,450 ppm for Cf-3 (1,485- to 1,502-m level), Wa-0 (1,520-m level), Wa-2 (1,665-m level), and Wa-2 (1,720-m level), respectively (Fig. 2*B* and Table 1).

The results for the modern GPP scenario agree well with other proxy data for the time slice between 50 and 60 Ma from $\delta^{13}C$ of paleosols (1, 36, 73), leaf stomata (36, 74–76), and $\delta^{13}C$ of marine phytoplankton (77), which nearly all range between 300 and 800 ppm (Fig. 2*B*). A few paleosol estimates propose a considerably lower pCO_2 of ∼100 ppm [ref. 78, reevaluated by Breecker et al. (73)], and a single estimate from $\delta^{13}C$ of fossil liverworts (79) suggests a considerably higher pCO_2 of ∼1,900 ppm for the Early Eocene.

Following Beerling and Royer (35), Paleocene and Eocene pCO_2 estimates from $\delta^{11}B$ of planktonic foraminifera were not considered for the present comparison due to several uncertainties (e.g., regarding diagenetic alteration and unknown vital effects of the analyzed foraminifera). Geochemical modeling (GEOCARBSULFvolc, refs. 80–82) predicts slightly higher pCO_2 than nearly all proxy results. However, the low resolution (10-Ma time steps) precludes tracking pCO_2 fluctuations within shorter time intervals.

Nearly all previously published proxy data represent either pre- or post-PETM estimates of pCO_2. Only Royer et al. [ref. 36, updated by Beerling et al. (76); compare also Beerling and Royer (35)] report a single stomatal index estimate revised to 670 ppm. This estimate is based on material from the Isle of Mull, United Kingdom, which was initially stated to correlate potentially to the PETM, within a data series of slightly older late Paleocene and younger early Eocene pCO_2 estimates ranging between 300 and 570 ppm.

Thus, the pCO_2 data presented here from the Wa-0 biozone, which to our knowledge are the first to track CO_2 levels directly through the CIE and PETM, are of particular interest and provide independent information on the potential carbon source generating the CIE.

Even when considering the large uncertainty in pCO_2 and a 2.3 times higher bioproductivity than today, all mean biozone estimates suggest a peak pCO_2 (upper error limit) not higher than about 2,500 ppm before and during the PETM and CIE, from Cf-3 to the start of Wa-2 (Fig. 2*B* and Table 1).

In the spectrum of pCO_2 values associated with different carbon sources considered as generating a global CIE in a range of –4 to –5‰, our results are compatible with dissociation of ∼2,500 to ∼4,500 Gt of highly ^{13}C-depleted marine methane clathrates, as initially proposed by Dickens et al. (29), which would require only a moderate pCO_2 increase (e.g., refs. 22, 24, and 27).

The model of Zeebe et al. (27) requires an increase in pCO_2 from a pre-PETM 1,000 ppm baseline to ∼1,700 ppm during the PETM main phase, based on an initial input of 3,000 Gt C from methane clathrates with a $\delta^{13}C$ lighter than –50‰. Furthermore, Zeebe et al. (27) claim that this 70% increase in pCO_2 is largely independent from the initial pre-PETM pCO_2, arguing for an increase from 500 to ∼850 ppm as likewise possible. A similar result was obtained by Cui et al. (24) when 2,500 Gt C from methane clathrates with a $\delta^{13}C$ of –60‰ was assumed as the potential carbon source (increase in pCO_2 from a baseline of 835 ppm to ∼1,500 ppm). In addition, the mass balance presented by McInerney and Wing (22) estimated a pCO_2 increase to ∼1,500 ppm, potentially triggered by a release of 4,300 Gt C from methane clathrates required to generate a CIE of –4.6‰. In a recent approach, Schubert and Jahren (83) calculated initial and peak-PETM CO_2 levels using the difference between the magnitude of the marine and terrestrial CIE (ΔCIE) and proposed a pCO_2 increase from 670 to 1,380 for the methane clathrate scenario.

All other sources in discussion for the CIE (thermogenic methane, permafrost soil carbon, carbon released due to wildfires or through desiccation and oxidation of organic matter due to drying of epicontinental seas as well as mantle CO_2) would have led to significantly higher CO_2 levels than suggested by our results.

If the observed CIE would have been induced by the release of thermogenic methane or permafrost soil carbon (10,000 Gt C, $\delta^{13}C$ ~–30‰), McInerney and Wing (22) proposed a pCO_2 increase to ~3,000 ppm. Using ΔCIE, Schubert and Jahren (83) calculated an increase from 920 to 2,480 ppm until the peak of the PETM for this scenario (Fig. 2). Such a scenario would still be within the uncertainty range of our data and cannot be completely excluded here.

Higher pCO_2 estimates have been proposed for carbon input from wildfires and/or desiccation and oxidation of organic matter from drying epicontinental seas (with a $\delta^{13}C$ of ~–22‰). The mass balance of McInerney and Wing (22) suggests CO_2 levels >4,000 ppm induced by a release of ~15,400 Gt of carbon. This is nearly identical to the model of Cui et al. (24), who proposed a release of 13,000 Gt C from the same source, resulting in a pCO_2 increase from 835 to 4,200 ppm. The proposed CO_2 concentrations are considerably higher than estimated from the present study.

An alternative model (25) suggests a minimum pulse of carbon with a $\delta^{13}C$ of –22‰ to be 6,800 Gt to trigger a CIE of –4‰, associated to an increase in pCO_2 to levels considerably above 2,000 ppm. The approach of Schubert and Jahren (83) suggests for the same carbon sources an increase from an initial value of 1,030 ppm to 3,340 ppm atmospheric CO_2 during the PETM.

Thus, the present study supports the initial idea of Dickens et al. (29) that massive releases of methane from clathrates caused the positive temperature excursion and the CIE during the PETM, at least to a considerable amount. Some criticisms to the methane clathrate scenario proposed in the last decade have turned out to be poorly constrained. One widely discussed argument is that pCO_2 values associated with the methane clathrate hypothesis are insufficient to explain the PETM temperature increase. However, alternative mechanisms, such as direct radiative forcing due to an increased pCH_4, and associated indirect effects (26, 27, 30, 31) may overrule this objection. The assumption that early Paleogene methane clathrate reservoirs were too small (84) has recently been discredited (26, 85). The idea that the amount of carbon released from methane clathrates would have been insufficient to explain observed shoaling of the carbonate compensation depth (86) has also been criticized (26). A massive release of CO_2 from soils, wildfires, or by oxidation of organic matter from drying epicontinental seas is not supported by the results of this study.

Conclusions

Triple oxygen isotope analysis of fossil mammalian bioapatite has the potential to trace fluctuations in temperature and CO_2 levels simultaneously, representing a powerful new tool for paleoclimatological research. Our *Ectocion* bioapatite data agree well with previous estimates of temperature change from the oxygen isotope composition of mammalian tooth enamel and from other proxies across the Paleocene–Eocene transition. Our results support existing proxy data for late Paleocene and early Eocene pCO_2. Our samples originate directly from pre-, peak- and post-PETM/CIE strata, making it possible for the first time to our knowledge to recognize any substantial change in CO_2 concentration within the respective time interval. Our data suggest that CO_2 levels during the PETM/CIE remained, within uncertainty of a few hundreds of parts per million, at pre- and post-PETM/CIE levels. Our data hence support the hypothesis that the CIE was mainly caused by a massive release of seabed methane to the atmosphere, and carbon emissions from other sources have made a subordinate contribution.

ACKNOWLEDGMENTS. We thank N. Albrecht, A. Höweling, C. Seidler, and M. Troche for assistance during sample pretreatment and isotope analysis; Verena Bendel for technical assistance in data analysis; Vanessa Roden, Wiebke Kallweit, and Tanja Stegemann for careful proofreading; and Reinhold Przybilla for technical support on the mass spectrometry line. A.G. was supported by German National Science Foundation Grant PA909/5-1 (to A.P.). Specimens analyzed here were collected with support from National Science Foundation Grant EAR-0125502 (to P.D.G.).

1. Koch P, Zachos JC, Gingerich PD (1992) Correlation between isotope records in marine and continental carbon reservoirs near the Palaeocene/Eocene boundary. *Nature* 358: 319–322.
2. Westerhold T, Röhl U, McCarren HK, Zachos JC (2009) Latest on the absolute age of the Paleocene-Eocene Thermal Maximum (PETM): New insights from exact stratigraphic position of key ash layers +19 and -17. *Earth Planet Sci Lett* 287(3):412–419.
3. Kennett JP, Stott LD (1991) Abrupt deep sea warming, palaeoceanographic changes and benthic extinctions at the end of the Palaeocene. *Nature* 353:225–229.
4. Aziz HA, et al. (2008) Astronomical climate control on paleosol stacking patterns in the upper Paleocene-lower Eocene Willwood Formation, Bighorn Basin, Wyoming. *Geology* 36(7):531–534.
5. Röhl U, Westerhold T, Bralower TJ, Zachos JC (2007) On the duration of the Paleocene-Eocene Thermal Maximum (PETM). *Geochem Geophys Geosyst* 8(12):Q12002.
6. Murphy BH, Farley KA, Zachos JC (2006) An extraterrestrial ^{3}He-based timescale for the Paleocene-Eocene Thermal Maximum (PETM) from Walvis Ridge, IODP Site 1266. *Geochim Cosmochim Acta* 74(17):5098–5108.
7. Farley KA, Eltgroth SF (2003) An alternative age model for the Paleocene-Eocene thermal maximum using extraterrestrial ^{3}He. *Earth Planet Sci Lett* 208(3):135–148.
8. Fricke HC, Wing SL (2004) Oxygen isotope and paleobotanical estimates of temperature and $\delta^{18}O$-latitude gradients over North America during the early Eocene. *Am J Sci* 304(7):612–635.
9. Zachos J, Pagani M, Sloan L, Thomas E, Billups K (2001) Trends, rhythms, and aberrations in global climate 65 Ma to present. *Science* 292(5517):686–693.
10. Zachos JC, et al. (2003) A transient rise in tropical sea surface temperature during the Paleocene-Eocene thermal maximum. *Science* 302(5650):1551–1554.
11. Tripati A, Elderfield H (2005) Deep-sea temperature and circulation changes at the Paleocene-Eocene Thermal Maximum. *Science* 308(5730):1894–1898.
12. Zachos JC, et al. (2006) Extreme warming of mid-latitude coastal ocean during the Paleocene-Eocene Thermal Maximum: Inferences from TEX_{86} and isotope data. *Geology* 34(9):737–740.
13. Thomas DJ, Zachos JC, Bralower TJ, Thomas E, Bohaty S (2002) Warming the fuel for the fire: Evidence for the thermal dissociation of methane hydrate during the Paleocene-Eocene thermal maximum. *Geology* 30(12):1067–1070.
14. Sluijs A, et al.; Expedition 302 Scientists (2006) Subtropical Arctic Ocean temperatures during the Palaeocene/Eocene thermal maximum. *Nature* 441(7093):610–613.
15. Weijers JWH, Schouten S, Sluijs A, Brinkhuis H, Sinninghe Damsté JS (2007) Warm arctic continents during the Palaeocene–Eocene thermal maximum. *Earth Planet Sci Lett* 261(1):230–238.
16. Bowen GJ, et al. (2001) Refined isotope stratigraphy across the continental Paleocene-Eocene boundary on Polecat Bench in the northern Bighorn Basin. *Paleocene-Eocene Stratigraphy and Biotic Change in the Bighorn and Clarks Fork Basins, Wyoming*, University of Michigan Papers on Paleontology, ed Gingerich PD (Museum of Paleontology, Univ of Michigan, Ann Arbor, MI), Vol 33, pp 73–78.
17. Fricke HC, Clyde WC, O'Neil JR, Gingerich PD (1998) Evidence for rapid climate change in North America during the latest Paleocene thermal maximum: Oxygen isotope compositions of biogenic phosphate from the Bighorn Basin (Wyoming). *Earth Planet Sci Lett* 160(1):193–208.
18. Koch PL, et al. (2003) Carbon and oxygen isotope records from paleosols spanning the Paleocene-Eocene boundary, Bighorn Basin, Wyoming. *Spec Pap Geol Soc Am* 369: 49–64.
19. Wing SL, et al. (2005) Transient floral change and rapid global warming at the Paleocene-Eocene boundary. *Science* 310(5750):993–996.
20. Secord R, Gingerich PD, Lohmann KC, Macleod KG (2010) Continental warming preceding the Palaeocene-Eocene thermal maximum. *Nature* 467(7318):955–958.
21. Koch P, Zachos JC, Dettmann DL (1995) Stable isotope stratigraphy and paleoclimatology of the Paleogene Bighorn Basin (Wyoming, USA). *Palaeogeogr Palaeoclimatol Palaeoecol* 115(1):61–89.
22. McInerney FA, Wing SL (2011) The Paleocene-Eocene Thermal Maximum: A perturbation of carbon cycle, climate, and biosphere with implications for the future. *Annu Rev Earth Planet Sci* 39:489–516.
23. Diefendorf AF, Mueller KE, Wing SL, Koch PL, Freeman KH (2010) Global patterns in leaf ^{13}C discrimination and implications for studies of past and future climate. *Proc Natl Acad Sci USA* 107(13):5738–5743.
24. Cui Y, et al. (2011) Slow release of fossil carbon during the Palaeocene-Eocene Thermal Maximum. *Nat Geosci* 4(7):481–485.
25. Panchuk K, Ridgwell A, Kump LR (2008) Sedimentary response to Paleocene-Eocene Thermal Maximum carbon release: A model-data comparison. *Geology* 36(4):315–318.
26. Dickens GR (2011) Down the rabbit hole: Toward appropriate discussion of methane release from gas hydrate systems during the Paleocene-Eocene thermal maximum and other past hyperthermal events. *Clim Past* 7(3):831–846.

27. Zeebe R, Zachos JC, Dickens GR (2009) Carbon dioxide forcing alone insufficient to explain Palaeocene-Eocene Thermal Maximum warming. *Nat Geosci* 2(8):576–580.
28. Higgins JA, Schrag DP (2006) Beyond methane: Towards a theory for the Paleocene-Eocene Thermal Maximum. *Earth Planet Sci Lett* 245(3):523–537.
29. Dickens GR, O'Neil JR, Rea DK, Owen RM (1995) Dissociation of oceanic methane hydrate as a cause of the carbon isotope excursion at the end of the Paleocene. *Paleoceanography* 10(6):965–971.
30. Kurtén T, et al. (2011) Large methane releases lead to strong aerosol forcing and reduced cloudiness. *Atmos Chem Phys* 11(14):6961–6969.
31. Schmidt GA, Shindell DT (2003) Atmospheric composition, radiative forcing, and climate change as a consequence of a massive methane release from gas hydrates. *Paleoceanography* 18(1):4-1–4-9.
32. Pagani M, Caldeira K, Archer D, Zachos JC (2006) Atmosphere. An ancient carbon mystery. *Science* 314(5805):1556–1557.
33. Renssen H, Beets J (2004) Modeling the climate response to a massive methane release from gas hydrates. *Paleoceanography* 19(2):PA2010.
34. Shellito CJ, Sloan LC, Huber M (2003) Climate model sensitivity to atmospheric CO_2 levels in the Early-Middle Paleogene. *Palaeogeogr Palaeoclimatol Palaeoecol* 193(1):113–123.
35. Beerling DJ, Royer DL (2011) Convergent Cenozoic CO_2 history. *Nat Geosci* 4(7): 418–420.
36. Royer DL, et al. (2001) Paleobotanical evidence for near present-day levels of atmospheric CO_2 during part of the tertiary. *Science* 292(5525):2310–2313.
37. Currano ED, et al. (2008) Sharply increased insect herbivory during the Paleocene-Eocene Thermal Maximum. *Proc Natl Acad Sci USA* 105(6):1960–1964.
38. Currano ED, Kattler KR, Flynn A (2011) Paleogene insect herbivory as a proxy for pCO_2 and ecosystem stress in the Bighorn Basin, Wyoming, USA. *Berichte der Geologischen Bundes-Anstalt* 85:61.
39. Longinelli A (1984) Oxygen isotopes in mammal bone phosphate: A new tool for paleohydrological and paleoclimatological research? *Geochim Cosmochim Acta* 48(2): 385–390.
40. Luz B, Kolodny Y, Horowitz M (1984) Fractionation of oxygen isotopes between mammalian bone phosphate and environmental drinking water. *Geochim Cosmochim Acta* 48(8):1689–1693.
41. Luz B, Kolodny Y (1985) Oxygen isotope variations in phosphate of biogenic apatites, IV. Mammal teeth and bones. *Earth Planet Sci Lett* 75(1):29–36.
42. Bryant JD, Froelich PN (1995) A model of oxygen isotope fractionation in body water of large mammals. *Geochim Cosmochim Acta* 59(21):4523–4537.
43. Kohn MJ (1996) Predicting animal $\delta^{18}O$: Accounting for diet and physiological adaption. *Geochim Cosmochim Acta* 60(23):4811–4829.
44. D'Angela D, Longinelli A (1990) Oxygen isotopes in living mammal's bone phosphate: Further results. *Chem Geol* 86(1):75–82.
45. Dansgaard W (1964) Stable isotopes in precipitation. *Tellus* 16(4):436–468.
46. Bryant JD, Luz B, Froelich PN (1994) Oxygen isotopic composition of fossil horse tooth phosphate as a record of continental paleoclimate. *Palaeogeogr Palaeoclimatol Palaeoecol* 107(3-4):303–316.
47. Sharp Z (2007) *Principles of Stable Isotope Geochemistry* (Prentice Hall, Upper Saddle River, NJ).
48. Luz B, Barkan E, Bender ML, Thiemens MH, Boering KA (1999) Triple-isotope composition of atmospheric oxygen as a tracer of biosphere productivity. *Nature* 400(6744):547–550.
49. Bao H, Lyons JR, Zhou C (2008) Triple oxygen isotope evidence for elevated CO_2 levels after a Neoproterozoic glaciation. *Nature* 453(7194):504–506.
50. Pack A, Gehler A, Süssenberger A (2013) Exploring the usability of isotopically anomalous oxygen in bones and teeth as paleo-CO_2-barometer. *Geochim Cosmochim Acta* 102:306–317.
51. Fricke HC (2003) Investigation of early Eocene water-vapor transport and paleoelevation using oxygen isotope data from geographically widespread mammal remains. *Geol Soc Am Bull* 115(9):1088–1096.
52. Secord R, Wing SL, Chew A (2008) Stable isotopes in Early Eocene mammals as indicators of forest canopy structure and resource partitioning. *Paleobiology* 34(2):282–300.
53. Secord R, et al. (2012) Evolution of the earliest horses driven by climate change in the Paleocene-Eocene Thermal Maximum. *Science* 335(6071):959–962.
54. Kohn MJ, Cerling TE (2002) Stable isotope compositions of biological apatite. *Rev Mineral Geochem* 48(1):455–488.
55. Gehler A, Tütken T, Pack A (2011) Triple oxygen isotope analysis of bioapatite as tracer for diagenetic alteration of bones and teeth. *Palaeogeogr Palaeoclimatol Palaeoecol* 310(1):84–91.
56. Gingerich PD, Smith T (2006) Paleocene-Eocene land mammals from three new latest Clarkforkian and earliest Wasatchian wash sites at Polecat Bench in the northern Bighorn Basin, Wyoming. Contributions from the Museum of Paleontology (Museum of Paleontology, Univ of Michigan, Ann Arbor, MI), Vol 31, pp 245–303.
57. Gingerich PD (1989) New earliest Wasatchian mammalian fauna from the Eocene of northwestern Wyoming: Composition and diversity in a rarely sampled high floodplain assemblage. University of Michigan Papers on Paleontology (Museum of Paleontology, Univ of Michigan, Ann Arbor, MI), Vol 28, pp 1–97.
58. Lindars ES, et al. (2001) Phosphate $\delta^{18}O$ determination of modern rodent teeth by direct laser fluorination: An appraisal of methodology and potential application to palaeoclimate reconstruction. *Geochim Cosmochim Acta* 65(15):2535–2548.
59. McKinney CR, McCrea JM, Epstein S, Allen HA, Urey HC (1950) Improvements in mass spectrometers for the measurement of small differences in isotope abundance ratios. *Rev Sci Instrum* 21(8):724–730.
60. Pack A, Herwartz D (2014) The triple oxygen isotope composition of the Earth mantle and understanding $\Delta^{17}O$ variations in terrestrial rocks and minerals. *Earth Planet Sci Lett* 390:138–145.
61. Sharp ZD (1990) A laser-based microanalytical method for the *in situ* determination of oxygen isotope ratios of silicates and oxides. *Geochim Cosmochim Acta* 54(5):1353–1357.
62. Pack A, Toulouse C, Przybilla R (2007) Determination of oxygen triple isotope ratios of silicates without cryogenic separation of NF_3- technique with application to analyses of technical O_2 gas and meteorite classification. *Rapid Commun Mass Spectrom* 21(22):3721–3728.
63. Asprey LB (1976) The preparation of very pure fluorine gas. *J Fluor Chem* 7(1):359–361.
64. Kohn MJ, Schoeninger MJ, Valley JW (1996) Herbivore tooth oxygen isotope compositions: Effects of diet and physiology. *Geochim Cosmochim Acta* 60(20):3889–3896.
65. Fricke HC, O'Neil JR (1999) The correlation between $^{18}O/^{16}O$ ratios of meteoric water and surface temperature: Its use in investigating terrestrial climate change over geologic time. *Earth Planet Sci Lett* 170(3):181–196.
66. Rozanski K, Araguás-Araguás L, Gonfiantini R (1993) Isotopic patterns in modern global precipitation. *Climate Change in Continental Isotope Records*, eds Swart PK, Lohmann KC, McKenzie J, Savin S (Am Geophysical Union, Washington, DC), pp 1–36.
67. Gourcy LL, Groening M, Aggarwal PK (1997) Stable oxygen and hydrogen isotopes in precipitation. *Isotopes in the Water Cycle: Past, Present and Future of a Developing Science*, eds Aggarwal PK, Gat JR, Froelich KFO (Springer, Dordrecht¸ The Netherlands), pp 39–51.
68. Rozanski K, Araguás-Araguás L, Gonfiantini R (1992) Relation between long-term trends of oxygen-18 isotope composition of precipitation and climate. *Science* 258(5084):981–985.
69. Gingerich PD (2003) Mammalian responses to climate change at the Paleocene-Eocene boundary: Polecat Bench record in the northern Bighorn Basin, Wyoming. *Causes and Consequences of Globally Warm Climates in the Early Paleogene*, eds Wing SL, Gingerich PD, Schmitz B, Thomas E, Geological Society of America Special Paper (Geological Soc of America, Boulder, CO), Vol 369, pp 463–478.
70. Gingerich PD (2006) Environment and evolution through the Paleocene-Eocene thermal maximum. *Trends Ecol Evol* 21(5):246–253.
71. Berner RA (2001) Modeling atmospheric O_2 over Phanerozoic time. *Geochim Cosmochim Acta* 65(5):685–694.
72. Beerling DJ (1999) Quantitative estimates of changes in marine and terrestrial primary productivity over the past 300 million years. *Proc Biol Sci* 266(1431):1821–1827.
73. Breecker DO, Sharp ZD, McFadden LD (2010) Atmospheric CO_2 concentrations during ancient greenhouse climates were similar to those predicted for A.D. 2100. *Proc Natl Acad Sci USA* 107(2):576–580.
74. Royer DL (2003) Estimating latest Cretaceous and Tertiary atmospheric CO_2 from stomatal indices. *Causes and Consequences of Globally Warm Climates in the Early Paleogene*, eds Wing SL, Gingerich PD, Schmitz B, Thomas E, Geological Society of America Special Paper (Geological Soc of America, Boulder, CO), Vol 369, pp 79–93.
75. Greenwood DR, Scarr MJ, Christophel DC (2003) Leaf stomatal frequency in the Australian tropical rainforest tree *Neolitsea dealbata* (Lauraceae) as a proxy measure of atmospheric pCO_2. *Palaeogeogr Palaeoclimatol Palaeoecol* 196(3):375–393.
76. Beerling DJ, Fox A, Anderson CW (2009) Quantitative uncertainty analyses of ancient atmospheric CO_2 estimates from fossil leaves. *Am J Sci* 309(9):775–787.
77. Stott LD (1992) Higher temperatures and lower oceanic pCO_2: A climate enigma at the end of the Paleocene epoch. *Paleoceanography* 7(4):395–404.
78. Sinha A, Stott LD (1994) New atmospheric pCO_2 estimates from paleosols during the late Paleocene/early Eocene global warming interval. *Global Planet Change* 9(3):297–307.
79. Fletcher BJ, Brentnall SJ, Anderson CW, Berner RA, Beerling DJ (2008) Atmospheric carbon dioxide linked with Mesozoic and early Cenozoic climate change. *Nat Geosci* 1(1):43–48.
80. Berner R (2006) GEOCARBSULF: A combined model for Phanerozoic atmospheric O_2 and CO_2. *Geochim Cosmochim Acta* 70(23):5653–5664.
81. Berner RA (2006) Inclusion of the weathering of volcanic rocks in the GEOCARBSULF model. *Am J Sci* 306(5):295–302.
82. Berner RA (2008) Addendum to "Inclusion of the weathering of volcanic rocks in the GEOCARBSULF model" (R. A. Berner, 2006, V. 306, p. 295–302). *Am J Sci* 308(1):100–103.
83. Schubert BA, Jahren AH (2013) Reconciliation of marine and terrestrial carbon isotope excursions based on changing atmospheric CO_2 levels. *Nat Commun* 4:1653.
84. Buffet B, Archer D (2004) Global inventory of methane clathrate: Sensitivity to changes in the deep ocean. *Earth Planet Sci Lett* 227(3):185–199.
85. Gu G, et al. (2011) Abundant Early Palaeogene marine gas hydrates despite warm deep-ocean temperatures. *Nat Geosci* 4(12):848–851.
86. Zachos JC, et al. (2005) Rapid acidification of the ocean during the Paleocene-Eocene thermal maximum. *Science* 308(5728):1611–1615.
87. Thiemens MH, Jackson T, Zipf E, Erdman PW, van Egmond C (1995) Carbon dioxide and oxygen isotope anomalies in the mesosphere and stratosphere. *Science* 339:780–785.
88. Barkan E, Luz B (2005) High precision measurements of $^{17}O/^{16}O$ and $^{18}O/^{16}O$ ratios in H_2O. *Rapid Commun Mass Spectrom* 19(24):3737–3742.
89. Barkan E, Luz B (2011) The relationships among the three stable isotopes of oxygen in air, seawater and marine photosynthesis. *Rapid Commun Mass Spectrom* 25(16):2367–2369.
90. Kaiser J, Abe O (2012) Reply to Nicholson's comment on "Consistent calculation of aquatic gross production from oxygen triple isotope measurements" by Kaiser (2011). *Biogeosciences* 9(8):2921–2933.
91. Young ED, Yeung LY, Kohl IE (2014) On the $\Delta^{17}O$ budget of atmospheric O_2. *Geochim Cosmochim Acta* 135:102–125.
92. Nagy KA, Peterson CC (1988) *Scaling of Water Flux Rate in Animals* (Univ of California Press, Berkeley, CA).
93. Nagy KA, Girard IA, Brown TK (1999) Energetics of free-ranging mammals, reptiles, and birds. *Annu Rev Nutr* 19(1):247–277.
94. Bao H, Koch PL, Rumble D, III (1999) Paleocene-Eocene climatic variation in western North America: Evidence from the $\delta^{18}O$ of pedogenic hematite. *Geol Soc Am Bull* 111(9):1405–1415.